DOI:
arXiv:1701.06799
http://doi.org/10.1063/1.4983990

Document Version
Publisher's PDF, also known as Version of record

Reciprocal space engineering with hyperuniform gold disordered surfaces

Marta Castro-Lopez, Michele Gaio, Steven Sellers, George Gkantzounis, Marian Florescu, and Riccardo Sapienza

Citation: APL Photonics **2**, 061302 (2017); doi: 10.1063/1.4983990
View online: http://dx.doi.org/10.1063/1.4983990
View Table of Contents: http://aip.scitation.org/toc/app/2/6
Published by the American Institute of Physics

Reciprocal space engineering with hyperuniform gold disordered surfaces

Marta Castro-Lopez,[1] Michele Gaio,[1] Steven Sellers,[2] George Gkantzounis,[2] Marian Florescu,[2,a] and Riccardo Sapienza[1,b]
[1]*Department of Physics, King's College London, Strand, London WC2R 2LS, United Kingdom*
[2]*Advanced Technology Institute and Department of Physics, University of Surrey, Guildford GU2 7XH, United Kingdom*

(Received 1 March 2017; accepted 9 May 2017; published online 26 May 2017)

Hyperuniform geometries feature correlated disordered topologies which follow from a tailored k-space design. Here, we study gold plasmonic hyperuniform disordered surfaces and, by momentum spectroscopy, we report evidence of k-space engineering on both light scattering and light emission. Even if the structures lack a well-defined periodicity, emission and scattering are directional in ring-shaped patterns. The opening of these rotational-symmetric patterns scales with the hyperuniform correlation length parameter as predicted via the spectral function method. [http://dx.doi.org/10.1063/1.4983990]

Coherent control of optical waves by scattering from 2D nanostructured surfaces is revolutionising the way we shape the wavefront of an incoming light beam, thus opening new avenues for miniaturised optical components for integrated optical circuits,[1] flat display technology,[2] and energy harvesting.[3,4] Metallic surfaces are in particular attractive due to the strong light-matter interaction associated with surface plasmons, enabling diffraction control through plasmonic crystals[5,6] and metal nano-particle arrays,[7,8] broadband operation and increase of the plasmon mode density,[9] enhanced omni-directional light extraction and coupling,[10] broadband absorption,[11] fluorescence enhancement[12] and lasing,[13,14] and more recently the realisation of ultra thin lenses[15] and metasurface holograms.[16]

Whereas periodic geometries suffer from limited rotational symmetries, aperiodic and disordered topologies, with their richer symmetries and patterns, can lead to superior optical functionalities,[8] as in omnidirectional absorption for solar applications,[17,18] scattering-induced light localisation,[19] and light extraction from the light emitting diodes (LED).[20] Moreover, disordered surfaces are expected to be more resilient against the fabrication imperfection and therefore more apt for the technological implementation. Given the vast possible designs of non-periodic topologies, ranging from random to correlated-disordered, their full potential is still to be fully explored.

There exists a general class of disordered systems, called hyperuniform disordered (HuD) photonic structures, which are of particular interest because they exhibit wide and isotropic photonic band gaps,[21,22] rotational symmetry, and broadband k-space control and can be systematically generated through a specific design rule via universal tessellation protocol.[23,24] Pioneering experiments on photonic HuD systems have explored IR light diffraction in 3D dielectric structures,[25] microwave band-gaps formation,[26] polarization filtering,[27] and random quantum cascade lasers.[28] Theoretical proposals have been put forward for surface enhanced Raman scattering,[29] transparency design,[30] high-Q optical cavities and low-loss waveguides,[31–33] and microwave photonic circuits.[26] HuD structures fabrication is improving quickly, reaching already the IR range[25] but not yet the visible.

[a]Electronic mail: m.florescu@surrey.ac.uk
[b]Electronic mail: riccardo.sapienza@kcl.ac.uk

Here, we report visible light scattering and light emission experiments from HuD plasmonic gold surfaces. We find that the scattering from these structures is principally directed into an annular angular pattern indicating reciprocal space engineering. Moreover, we investigate directional emission from near-field coupled emitters which, as confirmed by theoretical modelling, is shaped into a ring from the effective band folding into the light cone by scattering processes.

The HuD surfaces design is derived from a stealth hyperuniform point pattern with a stealthiness parameter $\chi = 0.49$, defined as the ratio between the number of constrained degrees of freedom to the total number of degrees of freedom, comprising 4000 points and generated under a periodic boundary condition, for a given average inter-scatterer distance a.[23] A section of the point pattern, decorated by discs of radius $0.3a$, is shown in Fig. 1(a). At $\chi = 0.49$, the hyperuniform point pattern exhibits significant local structural correlations. These structural correlations give rise to a highly constrained structure factor [shown in Fig. 1(b)] exhibiting a characteristic exclusion region for $0 \leq ak/2\pi \leq 0.73$ and a broad isotropic diffraction maximum peaked around $ak/2\pi = 1.03$.

Next, a Delaunay tessellation protocol[23] is performed, obtaining a strictly trivalent continuous network topology [Fig. 1(c)] with the walls of thickness $0.35a$. The structure factor of this network

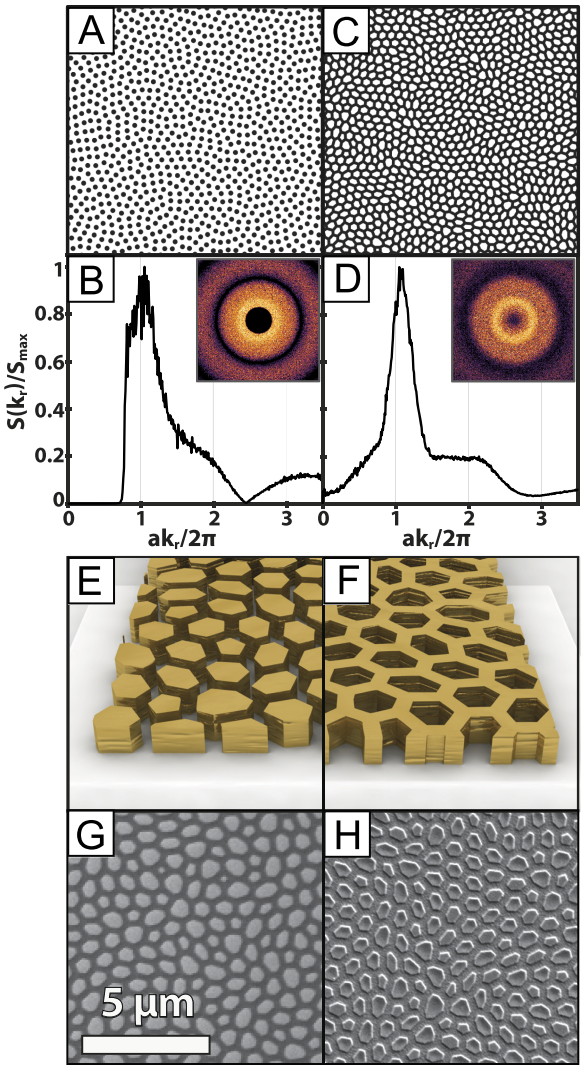

FIG. 1. The initial HuD point pattern [panel (a)] with χ = 0.49 presents a structure factor [panel (b)] with a typical zero around **k** = 0 and a broad isotropic diffraction maximum (inset). The HuD connected network [panel (c)] broadly preserves the **k**-space characteristics [panel (d)] of the point pattern. Sketches and SEM images of the resulting pillar-type [panels (e) and (g)] and network-type [panels (f) and (h)] HuD surfaces.

is presented in Fig. 1(d). The stealthiness of the architecture has been significantly reduced: the diffraction spectrum [Fig. 1(d), inset] exhibits low intensity diffuse scattering around $\mathbf{k} = 0$, in contrast to the sharp exclusion zone of the simple point pattern [Fig. 1(b), inset]. Nonetheless, the general form of the point pattern structure factor dominated by a single broad and isotropic resonance around $ak/2\pi = 1.09$ is reproduced by the network.

The hyperuniform designs are then converted into two families of metallic structures, a pillar-type structure comprising a connected air fraction enclosing isolated pentagonal, hexagonal, and heptagonal gold pillars and a network-type structure which is of inverted topology and consists of a connected network of gold enclosing isolated air pillars. An optimization is performed in the Fourier space[23] in order to design the scattering properties, resulting in both particles and waveguides having the variable shape and dimension. While in conventional plasmonic arrays, the building-block is chosen to be resonant to the lowest order plasmonic resonances, and it is therefore of diameter of the order of 10–100 nm, the pillars here, in a size range of 300–500 nm, support higher-order plasmonic modes resulting in a smearing out of the localised surface plasmon resonances. The same can be said of the waveguide geometry, whose width is around 300 nm, which supports a broad range of resonances. One can therefore expect that the main response of the metallic HuD surface is related to the structure factor, i.e., the diffraction from the nanostructured surface, with a broadband plasmonic contribution without a specific plasmon mode dominating. Therefore, strong similarities are expected between the optical response of the pillar-type and the network-type. A signature of the plasmonic dispersion is still present in the diffraction experiments and will be discussed later.

Gold HuD surfaces were fabricated by electron beam lithography on a glass substrate for various size scaling parameters a. The samples are of two kinds: *pillar-type* samples comprising isolated pentagonal, hexagonal, and heptagonal gold pillars [sketch in Fig. 1(e) and SEM in Fig. 1(g)], and *network-type* designs (identical but inverted) consisting of a connected network of gold [sketch in Fig. 1(f) and SEM in Fig. 1(h)]. The samples are labelled as L_pN for pillars and L_nN for networks, where $N = a \times \sqrt{4000}$ is the side dimension of the system: for example, L_p50 correspond to $a = 790$ nm and has a side dimension of 50 μm. Network designs larger or smaller than 40 μm have been cropped or periodically repeated, respectively, to cover a 40×40 μm^2 area.

Figure 2 presents light scattering experiments on the pillar-type HuD surfaces whose SEM images are shown in Fig. 2(a). Similar experiments performed on the network-type samples led to comparable results and are not shown here. The measured far-field intensity distribution of each pillar HuD surface is shown in Fig. 2(b). The samples were illuminated through the glass substrate with a circularly polarized collimated laser ($\lambda = 532$ nm), while the back-scattered light (unpolarized) was recorded in the far field by imaging the Fourier plane of a microscope objective (oil immersion, NA = 1.45). The maximum observable momenta are overlaid as a coloured dashed circle. All $L_p50 - L_p30$ samples exhibit broad and statistically isotropic scattering rings which resemble the primary resonance of the designed structure factor shown in the inset of Fig. 1(d). The momentum associated with the scattering resonance peak increases with the downscaling of the sample; in $L_p25 - L_p20$, the scattering ring crosses over the observable momentum limit. The bright spot at the centre of each far field results from the specular reflection along the axis of incidence.

Figure 2(c) shows the azimuthally averaged far-field intensity distributions. As the sample correlation length is reduced in size, the momentum of the primary scattering peak increases with a small intensity decrease. The structures $L_p50 - L_p35$ are all characterised by a single scattering peak with some finer structure that varies from sample to sample. Interestingly, the L_p30 sample exhibits a double peak, while L_p25 exhibits only a secondary low shoulder peak. The linear scaling with the reciprocal of the correlation length, shown in the insets of Fig. 2(c), can be expected by simple diffraction theory, while the finer structures are captured by numerical finite-difference time-domain (FDTD) simulations shown in Fig. 2(d). Our FDTD calculations were performed using a commercial software (Lumerical). We simulate only a small sub-region of the total 40 μm designs, for computational efficiency. The thickness of the samples was set to 45 nm. The size of the FDTD region was set to (22a + 5 μm, 22a + 5 μm, 1 μm) and was surrounded by perfectly matched layers. A minimum mesh size of 5 nm was used in the region close to the metal structures and a conformal mapping increased this number away from the metal region. Samples were illuminated by a total

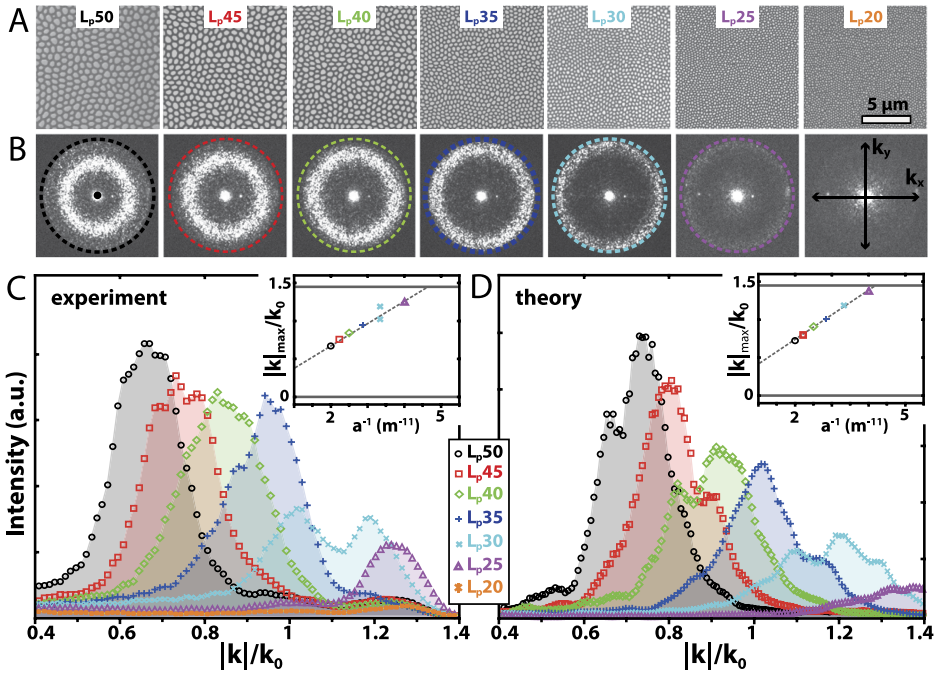

FIG. 2. SEM images of pillar type designs [panel (a)] together with their far-field diffraction patterns [panel (b)] when illuminated with a 532 nm laser. The numerical aperture limits are marked as coloured rings. Panel (c) displays the azimuthally integrated far-field distributions as a function of in-plane momentum (normalized to the incident wavevector k_0), showing broad scattering resonances. Panel (d) shows the same calculated azimuthally integrated far fields which agrees well with the experiment. The insets [panels (c) and (d)] plot the scattering peak position as a function of the reciprocal scaling parameter (a^{-1}) and the expected linear dependence.

field scattered field (TFSF) source producing circularly polarized plane waves of finite spatial extent for illumination either above or below the structure. We positioned a large planar detector at the metasurface/glass interface underneath the samples to record the near-field electric and magnetic fields. The near-field data recorded by this monitor was transformed to the far field. The glass substrate was simulated assuming a refractive index of 1.52 and Au using an available model based on experimental data.[34] In particular, FDTD predicts a multi-peak signature of the L_p30 sample, suggesting that this feature is a genuine property of the sample. We attribute this finer structure to the interplay of the surface plasmon at the air/gold interface sustained by a single pillar with the linear diffraction dispersion. In fact, the HuD structure comprises elements of different sizes, much larger than the plasmon wavelength, which present high-order resonances in the visible range and an overall response close to that of a surface plasmon resonance of an infinite film which peaks around $k/k_0 = 1.09$.

We performed also a broadband scattering characterization of the L_p50 design. The sample was illuminated from below with unpolarized white light, and the reflected and scattered light was spectrally decomposed into its wavelength and momentum components [Fig. 3(b)] by spectrally imaging the Fourier plane of the sample. In this way, an energy-wavevector dispersion diagram can be constructed as shown in Fig. 3(b) (experiments) and Fig. 3(a) (FDTD calculations). Both images display a bold diagonal slash, from low-scattering angle to high-scattering angle, and the evolution, for increasing wavelengths, towards larger momenta of the primary scattering peak. From this linear relationship, we conclude that the light diffraction follows the designed structure factor with a single main peak [Fig. 1(d)].

So far, we have investigated the ability of our gold HuD surfaces to mediate between the incident and scattered light. We now seek to characterise the HuD surface electromagnetic modes and their momentum distribution. The HuD surface modes are excited by a 50 nm layer of poly(methyl methacrylate) polymer highly doped with fluorescent 4-(dicyanomethylene)-2-methyl-6-(4-dimethylaminostyryl)-4H-pyran (DCM) dye molecules which was spin coated on the samples

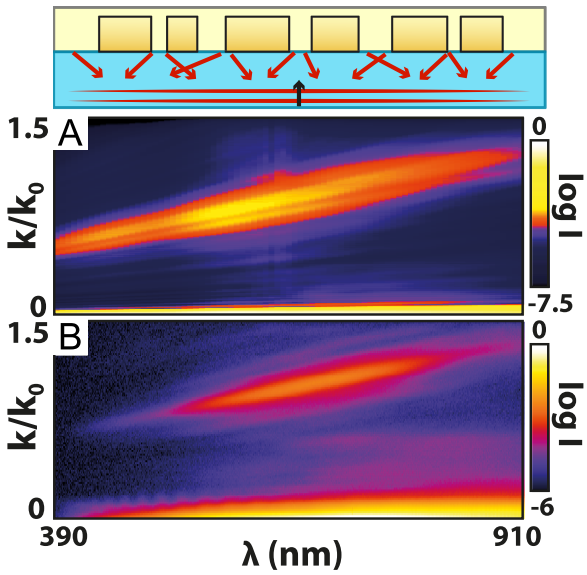

FIG. 3. Theoretical (a) and experimental (b) white light scattering by the L_p50 HuD surface. Both theory and experiment match well and show that the scattering peak momentum increases linearly with wavelength.

(Fig. 4, top panel). A fraction of the molecules, those closer (<10 nm) to the metal structures, will decay prevalently into plasmon excitations (with strong quenching), which will further outcouple to free space radiation. Increasing their distance from the metal, the molecules will instead radiate more and more into free-space modes (and minimal quenching), which will be scattered by the plasmonic structure.

Figures 4(a) and 4(b) present the theoretical and experimental frequency-momentum distribution, or dispersion plot, of the fluorescence light emitted from the L_p50 structure when excited with a circularly polarized green laser at a wavelength of 532 nm. The detection polarization was set along the spectrometer slit, to increase the signal to noise ratio. Figure 4(a) was obtained summing incoherently the far fields of 48 randomly oriented dipoles. The large number of dipoles introduced was sufficient to achieve convergence of the numerical results and robustness against different instances of the random distribution on their positions.

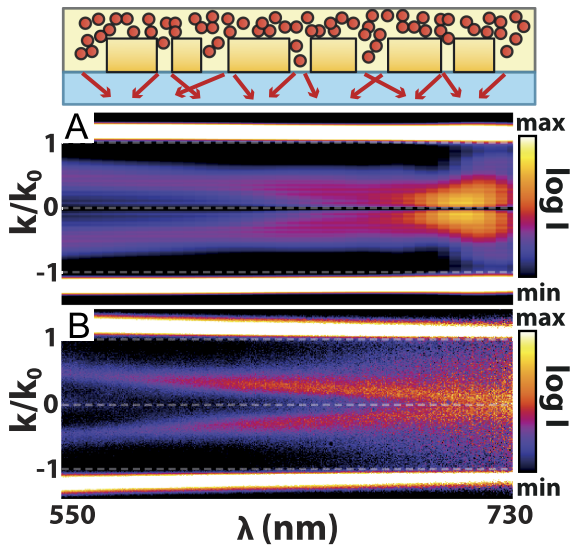

FIG. 4. Generalised dispersion relation $\omega(k)$ of L_p50 slab modes calculated summing incoherently the far fields of 48 randomly oriented dipole [panel (a)] and measured by fluorescence emission [panel (b)].

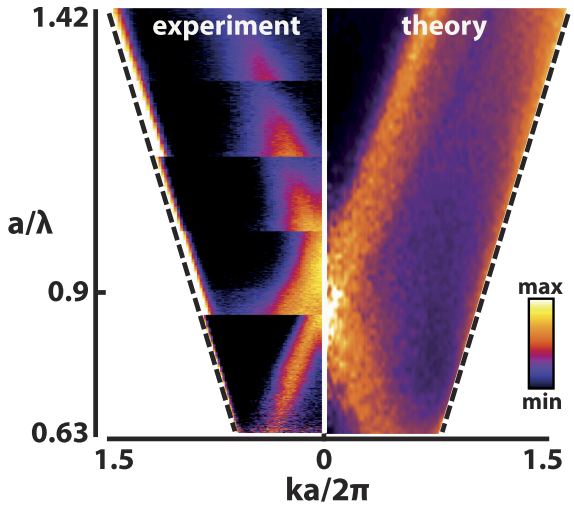

FIG. 5. Left: experimental dispersion relations for samples L_p50, L_p45, L_p40, L_p35, and L_p30 are stacked together as a function of a/λ. Right: FDTD simulations which confirm the crossing at $a/\lambda = 0.9$ where the light is emitted normal to the surface plane.

The pair of intense emission bands just outside the light lines (white dashed lines indicating $k/k_0 = \pm 1$) results from the characteristic radiation profile of a dipole near the glass-air interface.[35] Inside the light cone, we observe annular features which describe the decomposition of the HuD surface slab modes into their in-plane momentum components. These may be viewed as the generalised dispersion relation $\omega(\mathbf{k})$ of the slab modes. Similar dispersion diagrams were measured for the L_p50, L_p45, L_p40, L_p35, and L_p30 HuD surfaces.

In order to further analyse the dispersion plots of Fig. 4, we convert the emission wavelength and in-slab momentum to the dimensionless quantities a/λ and $ka/2\pi$, respectively. The experimental dispersion diagrams can then be stacked into a single image to illustrate the dispersion over a large normalized frequency range (Fig. 5, left panel). It shows that the fluorescent light is emitted isotropically from the HuD surface, into a cone with varying opening angles, which depends on the emission wavelength to correlation length ratio. As the frequency increases from $a/\lambda = 0.63$, the dominant momentum of the slab modes first decreases, reaching a zero in the region of $a/\lambda = 0.9$, at which point the light is emitted normal to the slab plane, before gradually opening back out. The experiments are in good agreement with FDTD calculations (Fig. 5, right panel) obtained with the spectral function method.[33] Specifically, the observed far-field angular profile can be understood as the coupling of the incident light to the slab eigenmodes. In a homogeneous structure, these eigenmodes lay outside the light cone and no coupling is possible. However, in a periodic crystal, the Bloch modes due to the 2D periodicity would enable the folding of this dispersion relation within the light cone and Bragg scattering would manifests itself in the far field. A similar mechanism happens in the present non-periodic case. Although no Bloch eigenmodes exist in the structure, multiple scattering occurring among the scatters leads to the formation of Bloch-like modes enabled from an averaged periodicity occurring due to the short-range order with a characteristic length, a. Similar to the periodic case, the structure factor is directly connected to the 2D Bloch-like modes that can be supported by our patterned structure. These modes enable the zone folding and identify this process as a Bragg-like process occurring in non-periodic structures. These results show that the electromagnetic dispersion diagram of the HuD surface follows the designed structure factor [Fig. 1(d)] and exhibits band folding resulting from the Bragg-like processes.

In conclusion, we designed, fabricated, and characterized gold HuD surfaces derived from HuD connected networks. Although lacking periodicity, by reciprocal space engineering, we designed the structure factor to be dominated by a single broad scattering resonance which was observed to dictate both the annular far-field light scattering and directional emission properties of the HuD surfaces. The observed HuD surface dispersion corresponds to an effective medium band that is back-folded by Bragg-like processes. Surface plasmon resonance was found to contribute to the diffraction by

inducing additional peaks from their interaction with the structural diffraction peak. The observed light emission and scattering engineering has important applications for light extraction from light-emitting devices, absorption in solar cells, albeit limited by metal losses, and annular redirection for displays, by exploiting the full azimuthal symmetry provided by the HuD surfaces design, when the light front is to be modified by a very thin optical component as for future imaging devices.

The work was supported by the Engineering and Physical Sciences Research Council (EPSRC Nos. EP/M027961/1 and EP/M013812/1), the Leverhulme Trust (No. RPG-2014-238), and the Royal Society (No. RG140457). This work was partially supported by the University of Surrey's IAA award to M.F., the EPSRC (United Kingdom) DTG Grant No. EP/J500562/1, EPSRC (United Kingdom) Strategic Equipment Grant No. EP/L02263X/1 (EP/M008576/1) and EPSRC (United Kingdom) Grant EP/M027791/1.

The data underlying the findings of this study are available without restriction.[36]

[1] B. Gholipour, J. Zhang, K. F. MacDonald, D. W. Hewak, and N. I. Zheludev, "An all-optical, non-volatile, bidirectional, phase-change meta-switch," Adv. Mater. **25**, 3050–3054 (2013).
[2] P. Hosseini, C. D. Wright, and H. Bhaskaran, "An optoelectronic framework enabled by low-dimensional phase-change films," Nature **511**, 206–211 (2014).
[3] A. K. Azad, W. J. M. Kort-Kamp, M. Sykora, N. R. Weisse-Bernstein, T. S. Luk, A. J. Taylor, D. A. R. Dalvit, and H.-T. Chen, "Metasurface broadband solar absorber," Sci. Rep. **6**, 20347 (2016).
[4] T. S. Almoneef and O. M. Ramahi, "Metamaterial electromagnetic energy harvester with near unity efficiency," Appl. Phys. Lett. **106**, 153902 (2015).
[5] W. L. Barnes, T. W. Preist, S. C. Kitson, J. R. Sambles, N. P. K. Cotter, and D. J. Nash, "Photonic gaps in the dispersion of surface plasmons on gratings," Phys. Rev. B **51**, 11164–11167 (1995).
[6] J.-S. Bouillard, P. Segovia, W. Dickson, G. A. Wurtz, and A. V. Zayats, "Shaping plasmon beams via the controlled illumination of finite-size plasmonic crystals," Sci. Rep. **4**, 7234 (2014).
[7] V. Giannini, G. Vecchi, and J. Gómez Rivas, "Lighting up multipolar surface plasmon polaritons by collective resonances in arrays of nanoantennas," Phys. Rev. Lett. **105**, 266801 (2010).
[8] L. Dal Negro and S. V. Boriskina, "Deterministic aperiodic nanostructures for photonics and plasmonics applications," Laser Photonics Rev. **6**, 178–218 (2012).
[9] S. M. Lubin, A. J. Hryn, M. D. Huntington, C. J. Engel, and T. W. Odom, "Quasiperiodic moiré plasmonic crystals," ACS Nano **7**, 11035–11042 (2013).
[10] N. Lawrence, J. Trevino, and L. Dal Negro, "Aperiodic arrays of active nanopillars for radiation engineering," J. Appl. Phys. **111**, 113101 (2012).
[11] F. Afshinmanesh, A. G. Curto, K. M. Milaninia, N. F. van Hulst, and M. L. Brongersma, "Transparent metallic fractal electrodes for semiconductor devices," Nano Lett. **14**, 5068–5074 (2014).
[12] M. Gaio, M. Castro-Lopez, J. Renger, N. van Hulst, and R. Sapienza, "Percolating plasmonic networks for light emission control," Faraday Discuss. **178**, 237–252 (2015).
[13] A. H. Schokker and A. F. Koenderink, "Statistics of randomized plasmonic lattice lasers," ACS Photonics **2**, 1289–1297 (2015).
[14] R. Zhang, S. Knitter, S. F. Liew, F. G. Omenetto, B. M. Reinhard, H. Cao, and L. Dal Negro, "Plasmon-enhanced random lasing in bio-compatible networks of cellulose nanofibers," Appl. Phys. Lett. **108**, 011103 (2016).
[15] N. Yu, P. Genevet, M. A. Kats, F. Aieta, J.-P. Tetienne, F. Capasso, and Z. Gaburro, "Light propagation with phase discontinuities: Generalized laws of reflection and refraction," Science **334**, 333–337 (2011).
[16] X. Ni, A. V. Kildishev, and V. M. Shalaev, "Metasurface holograms for visible light," Nat. Commun. **4**, 2807 (2013).
[17] E. R. Martins, J. Li, Y. Liu, V. Depauw, Z. Chen, J. Zhou, and T. F. Krauss, "Deterministic quasi-random nanostructures for photon control," Nat. Commun. **4**, 2665 (2013).
[18] M. Burresi, F. Pratesi, K. Vynck, M. Prasciolu, M. Tormen, and D. S. Wiersma, "Two-dimensional disorder for broadband, omnidirectional and polarization-insensitive absorption," Opt. Express **21**, A268–A275 (2013).
[19] A. Lagendijk, B. van Tiggelen, and D. S. Wiersma, "Fifty years of Anderson localization," Phys. Today **62**(8), 24–29 (2009).
[20] W. H. Koo, S. M. Jeong, F. Araoka, K. Ishikawa, S. Nishimura, T. Toyooka, and H. Takezoe, "Light extraction from organic light-emitting diodes enhanced by spontaneously formed buckles," Nat. Photonics **4**, 222–226 (2010).
[21] L. S. Froufe-Pérez, M. Engel, P. F. Damasceno, N. Muller, J. Haberko, S. C. Glotzer, and F. Scheffold, "Role of short-range order and hyperuniformity in the formation of band gaps in disordered photonic materials," Phys. Rev. Lett. **117**, 053902 (2016).
[22] L. S. Froufe-Pérez, M. Engel, J. J. Sáenz, and F. Scheffold, "Transport phase diagram and Anderson localization in hyperuniform disordered photonic materials," e-print arXiv:1702.03883 (2017), pp. 1–14.
[23] M. Florescu, S. Torquato, and P. J. Steinhardt, "Designer disordered materials with large, complete photonic band gaps," Proc. Natl. Acad. Sci. U. S. A. **106**, 20658–20663 (2009).
[24] M. Florescu, S. Torquato, and P. J. Steinhardt, "Complete band gaps in two-dimensional photonic quasicrystals," Phys. Rev. B **80**, 155112 (2009).
[25] N. Muller, J. Haberko, C. Marichy, and F. Scheffold, "Silicon hyperuniform disordered photonic materials with a pronounced gap in the shortwave infrared," Adv. Opt. Mater. **2**, 115–119 (2014).

[26] W. Man, M. Florescu, E. P. Williamson, Y. He, S. R. Hashemizad, B. Y. C. Leung, D. R. Liner, S. Torquato, P. M. Chaikin, and P. J. Steinhardt, "Isotropic band gaps and freeform waveguides observed in hyperuniform disordered photonic solids," Proc. Natl. Acad. Sci. U. S. A. **110**, 15886–15891 (2013).
[27] W. Zhou, Z. Cheng, B. Zhu, X. Sun, and H. K. Tsang, "Hyperuniform disordered network polarizers," IEEE J. Sel. Top. Quantum Electron. **22**, 288–294 (2016).
[28] R. Degl'Innocenti, Y. D. Shah, L. Masini, A. Ronzani, A. Pitanti, Y. Ren, D. S. Jessop, A. Tredicucci, H. E. Beere, and D. A. Ritchie, "Hyperuniform disordered terahertz quantum cascade laser," Sci. Rep. **6**, 19325 (2016).
[29] C. De Rosa, F. Auriemma, C. Diletto, R. Di Girolamo, A. Malafronte, P. Morvillo, G. Zito, G. Rusciano, G. Pesce, and A. Sasso, "Toward hyperuniform disordered plasmonic nanostructures for reproducible surface-enhanced Raman spectroscopy," Phys. Chem. Chem. Phys. **17**, 8061–8069 (2015).
[30] O. Leseur, R. Pierrat, and R. Carminati, "High-density hyperuniform materials can be transparent," Optica **3**, 763 (2016).
[31] M. Florescu, P. J. Steinhardt, and S. Torquato, "Optical cavities and waveguides in hyperuniform disordered photonic solids," Phys. Rev. B **87**, 165116 (2013).
[32] T. Amoah and M. Florescu, "High-Q optical cavities in hyperuniform disordered materials," Phys. Rev. B **91**, 020201 (2015); e-print arXiv:1504.07055.
[33] S. Tsitrin, E. P. Williamson, T. Amoah, G. Nahal, H. L. Chan, M. Florescu, and W. Man, "Unfolding the band structure of non-crystalline photonic band gap materials," Sci. Rep. **5**, 13301 (2015).
[34] P. B. Johnson and R. W. Christy, "Optical constants of the noble metals," Phys. Rev. B **6**, 4370–4379 (1972).
[35] L. Novotny, *Principles of Nano-Optics* (Cambridge University Press, Cambridge, UK, 2006), e-print arXiv:1011.1669v3.
[36] M. Castro-Lopez, M. Gaio, S. Sellers, G. Gkantzounis, M. Florescu, and R. Sapienza, "Reciprocal space engineering with hyperuniform gold disordered surfaces," Figshare (2017).